NOTES AND CORRESPONDENCE

Compressible Flow Simulations on Numerically Generated Grids

By Takehiko Satomura

Meteorological Research Institute, 1-1, Nagamine, Tsukuba, Ibaraki 305, Japan
(Manuscript received 21 December 1988, in revised form 13 April 1989)

1. Introduction

Recently, more frequent numerical experiments of flow over complex terrain have been performed. In such simulations, the Cartesian system represents the effects of the curved boundary unsatisfactorily, since it resolves the slope of the boundary into steps. It has therefore been considered that a solution to this problem is a coordinate transformation such that a coordinate surface or a curve follows the boundary. On the other hand, use of an orthogonal system is more desirable than a non-orthogonal system because the truncation error increases with the departure from orthogonality. We can construct two-dimensional coordinate systems which satisfy the above two conditions: the orthogonality and the coincidence with the boundary shape (for example, Sahasi 1981; Ryskin and Leal 1983; Sharman *et al.*, 1988). In three dimensions, however, we cannot generate orthogonal systems which follow an arbitrary boundary shape (Eiseman, 1982). A practical solution of the boundary problem is then to generate non-orthogonal (but not far away from the orthogonality) coordinates whose coordinate surfaces fit given boundaries.

In meteorological numerical simulations, two transformations of the vertical coordinate have been widely used: the z* coordinates introduced by Gal-Chen and Somerville (1975) and the σ coordinates proposed by Phillips (1957). In z* coordinates, only the vertical coordinate is transformed to fit the lower boundary (*i.e.*, the terrain) and, in the σ coordinates, the vertical coordinate is replaced by the hydrostatic pressure normalized by the surface pressure. These are terrain-following coordinates, but the coordinate lines emitted from the terrain are vertical. They have, therefore, the disadvantage that finite-difference error would be large over the steep terrain.

Aeronautical engineers have developed techniques which generate grid points with desired characteristics around objects of complex shape. An extensive review was given on this subject by Thompson *et al.* (1982) and by Thompson (1984). Using these techniques, we can generate coordinate lines which start from the three-dimensional boundary nearly at right angles. In this paper, one of these generation techniques, called a variational grid generation, will be adapted to mountain-wave simulations and some preliminary results will be shown.

The geometric transformation introduced to simplify the boundary condition changes the governing equations into complicated forms. The Poisson equation which diagnostically determines the pressure in the anelastic systems is also complicated (*e.g.*, Clark, 1977) and direct Poisson solvers are impractical. This latter point obliges us to use iterative solvers which consume much computer time. We will therefore use the elastic systems as basic equations as shown in the next section. In addition, it will be shown that we can simplify the equations by choosing Cartesian velocity as dependent variables. The numerical grid generation method, which was proposed by Brackbill and Saltzman (1982), will be described in section 3. The results of numerical experiments will be shown in section 4. The detailed numerical schemes will be found in appendix.

2. Model equations

We confine the analysis of the present article to two-dimensional coordinates for simplicity of presentation. The technique employed herein is easily extended to three dimensions.

a. Cartesian systems

The momentum, thermodynamic and continuity equations may be written in two dimensions as follows:

$$\frac{\partial u}{\partial t} + u\frac{\partial u}{\partial x} + w\frac{\partial u}{\partial z} + c_p(\Theta + \theta)\frac{\partial \pi}{\partial x} = F_u, \qquad (2.1)$$

$$\frac{\partial w}{\partial t} + u\frac{\partial w}{\partial x} + w\frac{\partial w}{\partial z}$$

$$+ \quad c_p(\Theta+\theta)\frac{\partial \pi}{\partial z} - g\frac{\theta}{\Theta} = F_w, \tag{2.2}$$

$$\frac{\partial \theta}{\partial t} + u\frac{\partial \theta}{\partial x} + w\frac{\partial \theta}{\partial z} = F_\theta, \tag{2.3}$$

$$\begin{aligned}\frac{\partial \pi}{\partial t} &+ u\frac{\partial \pi}{\partial x} + w\frac{\partial}{\partial z}(\Pi+\pi)\\ &+ \frac{R_d(\Pi+\pi)}{c_v}\left(\frac{\partial u}{\partial x}+\frac{\partial w}{\partial z}\right)\\ &= \frac{R_d(\Pi+\pi)}{c_v(\Theta+\theta)}F_\theta,\end{aligned} \tag{2.4}$$

where

$$\Pi+\pi = \left(\frac{p}{p_o}\right)^{R_d/c_p}, \tag{2.5}$$

and

$$\frac{d\Pi}{dz} = -\frac{g}{c_p\Theta} = -\frac{1}{H_s}. \tag{2.6}$$

In the above, p is the pressure, p_o=10^5 Pa, R_d is the gas constant for dry air, c_p and c_v are the specific heat of dry air at constant pressure and at constant volume respectively, (u, w) are the velocity components in the x (horizontal) and z (vertical) directions respectively, θ is the potential temperature deviation from a constant value Θ.

The right-hand-sides of (2.1)-(2.4) are the contributions from turbulent mixing, for which we employ a conventional first-order closure formulation (Lilly, 1962) as:

$$F_u = \frac{\partial}{\partial x}(K_M A) + \frac{\partial}{\partial z}(K_M B), \tag{2.7}$$

$$F_w = \frac{\partial}{\partial x}(K_M B) - \frac{\partial}{\partial z}(K_M A), \tag{2.8}$$

$$F_\theta = \frac{\partial}{\partial x}\left(K_H\frac{\partial \theta}{\partial x}\right) - \frac{\partial}{\partial z}\left(K_H\frac{\partial \theta}{\partial z}\right), \tag{2.9}$$

where

$$A = \left(\frac{\partial u}{\partial x} - \frac{\partial w}{\partial z}\right), \quad B = \left(\frac{\partial u}{\partial z} + \frac{\partial w}{\partial x}\right), \tag{2.10}$$

$$\begin{aligned}K_M &= k^2\Delta x\Delta z\,(A^2+B^2)^{1/2}\\ &\times \left[\max\left(1-\frac{K_H}{K_M}Ri, 0\right)\right]^{1/2},\end{aligned} \tag{2.11}$$

$$Ri = \frac{N^2}{A^2+B^2}, \tag{2.12}$$

k=0.25 (Clark, 1977), and K_H/K_M=3 (Deardorff, 1972).

b. Curvilinear systems

Terrain can be incorporated in the model by a transformation from Cartesian coordinates (x,z) to curvilinear coordinates (ξ, ζ),

$$\begin{cases} x = x\,(\xi,\zeta) \\ z = z\,(\xi,\zeta)\,. \end{cases} \tag{2.13}$$

Transformation formulae in the general case are provided in standard texts and papers: for example, Pielke (1984, Ch. 6), Thompson *et al.* (1985), Gal-Chen and Somerville (1975) and Sharman *et al.* (1988). It is noteworthy that, if the basic equations (2.1)–(2.4) are transformed straightforwardly, metric terms complicate the transformed equations and second derivatives of the coordinate variables appear in them. These terms would increase the finite-difference error and the round-off error. The general representation of the anelastic momentum equations can be, however, reduced to a simpler form when the Cartesian dependent velocity (u,w) is retained in some parts of the transformed equations as, for example, in Clark (1977). Fortunately, the elastic system is also simplified in the same manner as follows:

$$\begin{aligned}\frac{\partial u}{\partial t} &+ \hat{u}\frac{\partial u}{\partial \xi} + \hat{w}\frac{\partial u}{\partial \zeta}\\ &+ c_p(\Theta+\theta)\left(\frac{\partial \xi}{\partial x}\frac{\partial \pi}{\partial \xi} + \frac{\partial \zeta}{\partial x}\frac{\partial \pi}{\partial \zeta}\right) = F_u,\end{aligned} \tag{2.14}$$

$$\begin{aligned}\frac{\partial w}{\partial t} &+ \hat{u}\frac{\partial w}{\partial \xi} + \hat{w}\frac{\partial w}{\partial \zeta}\\ &+ c_p(\Theta+\theta)\left(\frac{\partial \xi}{\partial z}\frac{\partial \pi}{\partial \xi} + \frac{\partial \zeta}{\partial z}\frac{\partial \pi}{\partial \zeta}\right)\\ &- g\frac{\theta}{\Theta} = F_w,\end{aligned} \tag{2.15}$$

$$\frac{\partial \theta}{\partial t} + \hat{u}\frac{\partial \theta}{\partial \xi} + \hat{w}\frac{\partial \theta}{\partial \zeta} = F_\theta, \tag{2.16}$$

$$\begin{aligned}\frac{\partial \pi}{\partial t} &+ \hat{u}\frac{\partial \pi}{\partial \xi} + \hat{w}\frac{\partial \pi}{\partial \zeta} - \frac{w}{H_s}\\ &+ \frac{R_d(\Pi+\pi)}{c_v}\left(\frac{\partial \xi}{\partial x}\frac{\partial u}{\partial \xi} + \frac{\partial \zeta}{\partial x}\frac{\partial u}{\partial \zeta}\right.\\ &\left.+ \frac{\partial \xi}{\partial z}\frac{\partial w}{\partial \xi} + \frac{\partial \zeta}{\partial z}\frac{\partial w}{\partial \zeta}\right)\\ &= \frac{R_d(\Pi+\pi)}{c_v(\Theta+\theta)}F_\theta,\end{aligned} \tag{2.17}$$

where $(\hat{u}, \hat{w})$ are the contravariant components of the velocity in the transformed base vectors and (u, w) are the Cartesian velocity using (ξ, ζ) as independent variables.

Given the transformation function (2.13), the governing equations (2.14)–(2.17) are solved numerically. For practical purposes, however, we need not know the functional form of the transformation (2.13). It is sufficient that grid positions are known

in both the Cartesian and the curvilinear coordinates, because we approximate the metric terms by finite differences.

3. Numerical grid generation

We use the grid generation technique formulated as a variational problem. This formulation was proposed by Brackbill and Saltzman (1982) and is represented here for readers' convenience. Please refer to the original paper for detail.

Define three integrals as measures of global smoothness of the transformation I_s, orthogonality I_o, and weighted volume variation I_v:

$$I_s = \int_D \{(\nabla\xi)^2 + (\nabla\zeta)^2\} dD, \tag{3.1}$$

$$I_o = \int_D (\nabla\xi \cdot \nabla\zeta)^2 J^3 dD, \tag{3.2}$$

$$I_v = \int_D \boldsymbol{w} J dD, \tag{3.3}$$

where $\boldsymbol{w}=\boldsymbol{w}(x,y)$ is a given weight function that determines the variation of the cell volume and

$$J = \frac{\partial x}{\partial \xi}\frac{\partial z}{\partial \zeta} - \frac{\partial x}{\partial \zeta}\frac{\partial z}{\partial \xi}. \tag{3.4}$$

The integral to be minimized is

$$\begin{aligned} I &= I_s + \frac{\lambda_v I_v}{\boldsymbol{W}\cdot \Delta L^4} + \frac{\lambda_o I_o}{\Delta L^4} \\ &= I_s + \lambda_v' I_v + \lambda_o' I_o, \end{aligned} \tag{3.5}$$

where

$$\boldsymbol{W} = \frac{\int_D \boldsymbol{w} dD}{\int_D dD},$$

λ_v and λ_o are parameters of relative importance of the three properties, ΔL is a characteristic grid length. The term ΔL^{-4} in (3.5) is introduced to match the order of each of the integral indices (Thompson *et al.* 1985, Ch. 11).

The Euler equations of (3.5) are

$$\begin{aligned} b_1\frac{\partial^2 x}{\partial \xi^2} &+ b_2\frac{\partial^2 x}{\partial \xi \partial \zeta} + b_3\frac{\partial^2 x}{\partial \zeta^2} \\ &+ a_1\frac{\partial^2 z}{\partial \xi^2} + a_2\frac{\partial^2 z}{\partial \xi \partial \zeta} + a_3\frac{\partial^2 z}{\partial \zeta^2} \\ &+ \frac{J^2}{2}\frac{\partial \boldsymbol{w}}{\partial x}\lambda_v = 0 \end{aligned} \tag{3.6}$$

$$\begin{aligned} a_1\frac{\partial^2 x}{\partial \xi^2} &+ a_2\frac{\partial^2 x}{\partial \xi \partial \zeta} + a_3\frac{\partial^2 x}{\partial \zeta^2} \\ &+ c_1\frac{\partial^2 z}{\partial \xi^2} + c_2\frac{\partial^2 z}{\partial \xi \partial \zeta} + c_3\frac{\partial^2 z}{\partial \zeta^2} \\ &+ \frac{J^2}{2}\frac{\partial \boldsymbol{w}}{\partial z}\lambda_v = 0 \end{aligned} \tag{3.7}$$

where the coefficients a_i, b_i and c_i (i=1,3) are functions of first order derivatives of λ_v', λ_o', $x(\xi, \zeta)$ and/or $z(\xi, \zeta)$. By replacing the differential with centered finite difference, (3.6) and (3.7) can be solved by a simple iterative method with appropriate boundary conditions. In the following, we fix grid points on the lower boundary and apply the orthogonal condition at other boundaries.

4. Examples of flow simulations

In this section, we will show some results of flow simulation for two-dimensional mountain waves both in non-hydrostatic and in hydrostatic regimes. These examples were chosen because they have been widely studied using both numerical and analytical approaches and results are available for comparison.

In the present numerical model, a centered finite difference scheme in space and time is used. A semi-implicit time scheme is also used for acoustic terms in the ζ-direction to save computer time. The horizontal boundaries of the model are open: the radiation condition of Orlanski (1976) for the normal velocity, u, and zero normal derivative for the other variables. At the top and the bottom, the "rigid and free-slip" condition is imposed. A "sponge" layer, following the analysis of Klemp and Lilly (1978), is inserted above the 10km level to reduce reflection from the top boundary.

In the following, we will show two types of experiments. The first was simulations of flow over a bell-shaped low mountain embedded in a homogeneous atmosphere. The purpose of these experiments was to test the ability to reproduce linear solutions. The second type of experiment was conducted in two different coordinates for flow over a mountain with cliffs. This second type would show differences between coordinate transformations.

Figures 1a and 2a display vertical velocity fields in flow over a bell-shaped mountain,

$$z_s = \frac{ha^2}{(x-x_o)^2 + a^2}, \tag{4.1}$$

where z_s is the surface elevation, x_o is the center of the mountain, with half-widths a=1km and 10km, respectively. In both cases, the mountain height h=10m, the atmosphere is isothermal (T_B=300 K), and the Scorer parameter is $10^{-3}\mathrm{m}^{-1}$. The typical wave propagation pattern is represented well in both figures, and they are in good agreement with the analytical linear solutions shown in Figs. 1b and 2b, respectively.

In the case where the slope of the terrain is gentle as in Figs.1 and 2, the flow simulated in the generated grid system shows no apparent difference from that in z* system which is widely used by meteorologists:

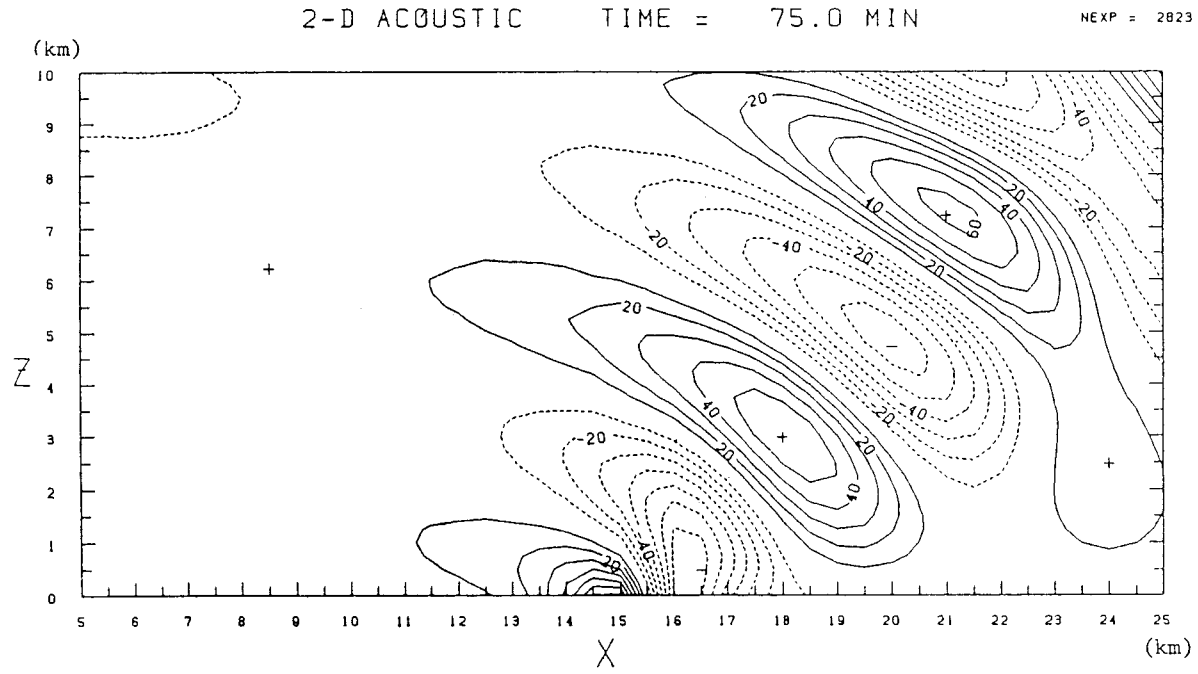

Fig. 1a. Contours of simulated vertical velocity for stratified flow over the bell-shaped mountain with a half-width of 1 km and a height 10 m. The unit of velocity is 0.1 cm/sec.

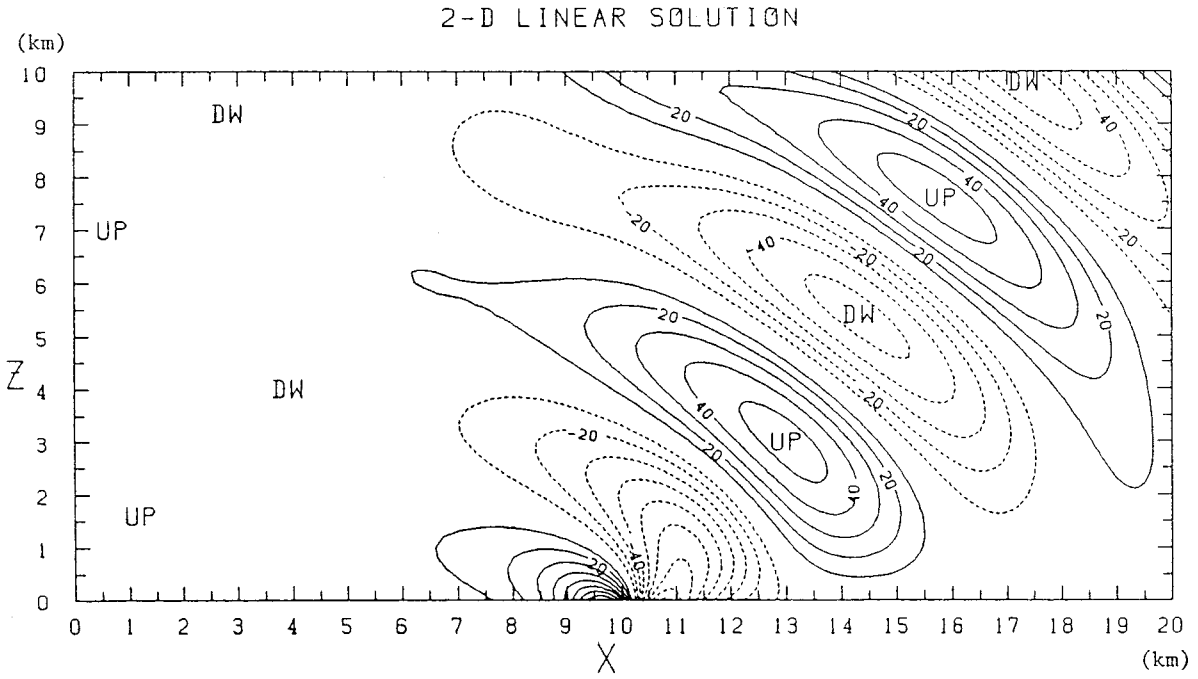

Fig. 1b. As in Fig. 1a, except the analytical linear solution.

$$\begin{cases} x^* = x \\ z^* = z_T \dfrac{z - z_s}{z_T - z_s}, \end{cases} \tag{4.2}$$

where z_T is the height of the model top. In the case where the slope of the mountain is steep, however, the difference between the above two-coordinate systems will be evident. In order to show the difference in an extreme example, simulations of flow over a semi-circular mountain were conducted in the two coordinates. The transformed grids and simulated vertical velocity are shown in Figs. 3 and 4 for the generated and z* coordinates, respectively. In both

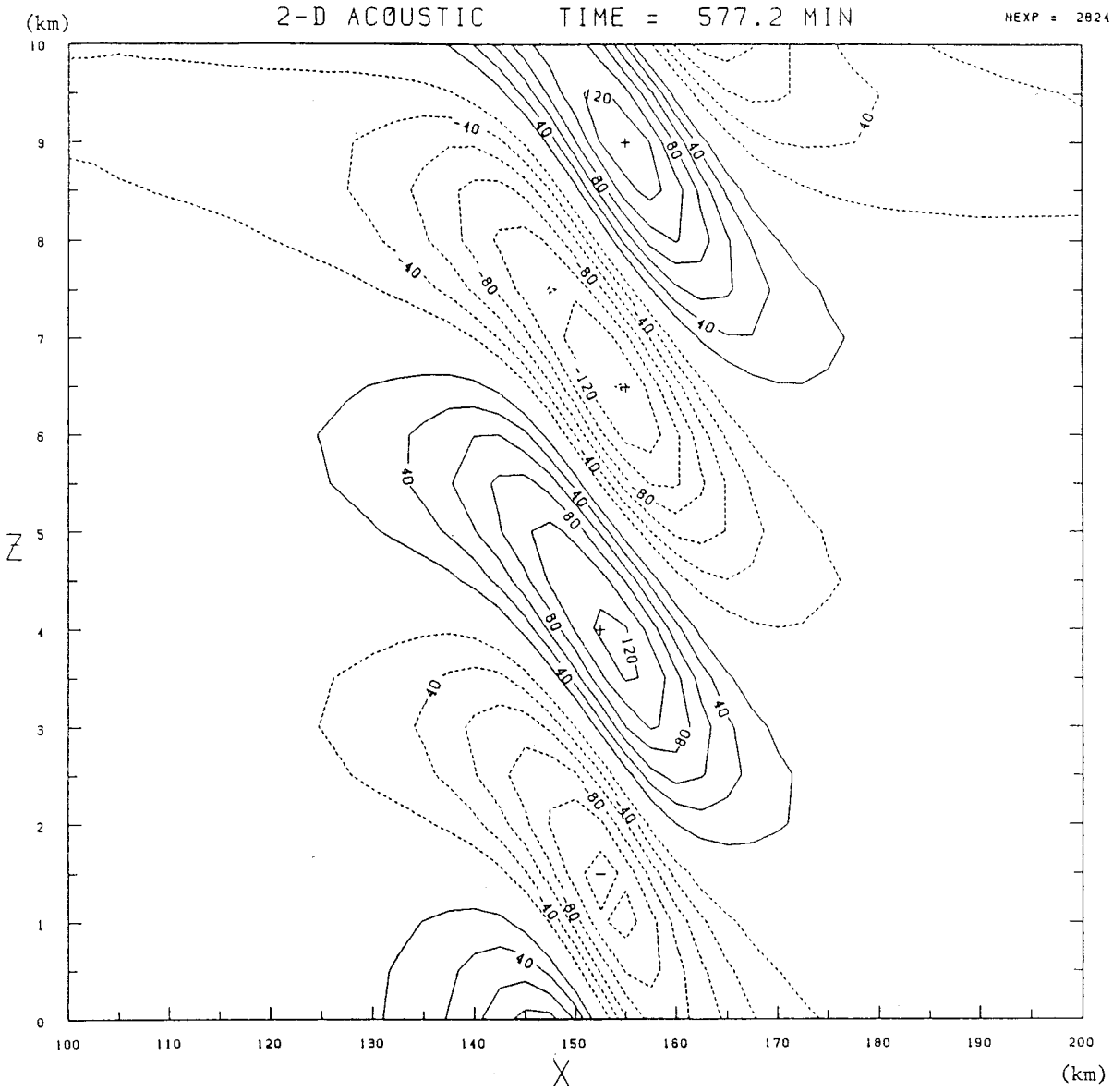

Fig. 2a. As in Fig. 1a, except that the half width of the mountain is 10 km.

figures, the radius of the mountain is 1km, the atmosphere has a constant Brunt-Väisälä frequency $N=10^{-2}sec^{-1}$, and the Froude number Fr=U/Nh is unity. These conditions coincide with Fig. A2 of Miles and Huppert (1968) who derived the analytical solution of Long's equation (Long 1955).

Comparing Figs. 3 and 4, we see clearly that spurious vertical velocity modes appear just above the mountain in the z* coordinates. Because the truncation error increases inversely with the sine of the angle between the coordinate lines (Thompson *et al.* 1985, Ch. 5), this erroneous vertical velocity is considered to originate in that error due to the departure of the z* coordinates (4.2) from orthogonality. The generated coordinates are, on the other hand, more orthogonal than the z*coordinates, and little spurious velocity is seen in Fig. 3.

5. Summary and discussion

We have adapted a variational grid generation technique to mountain-wave simulations and have shown that the simulated waves over the low mountains are in good agreement with linear theory. It is also shown that in the generated grid systems the flow over the steep mountain can be simulated without a large finite-difference error compared to that found in the z* coordinates.

The finite-difference schemes we used conserve neither total energy nor momentum, although it is desirable to use schemes which satisfy conservation laws. The non-conservation characteristics of our schemes are not considered to introduce serious error into the simulated results because total energy changed only 0.3 % during the time integration of the linear mountain-wave cases. It is also difficult in

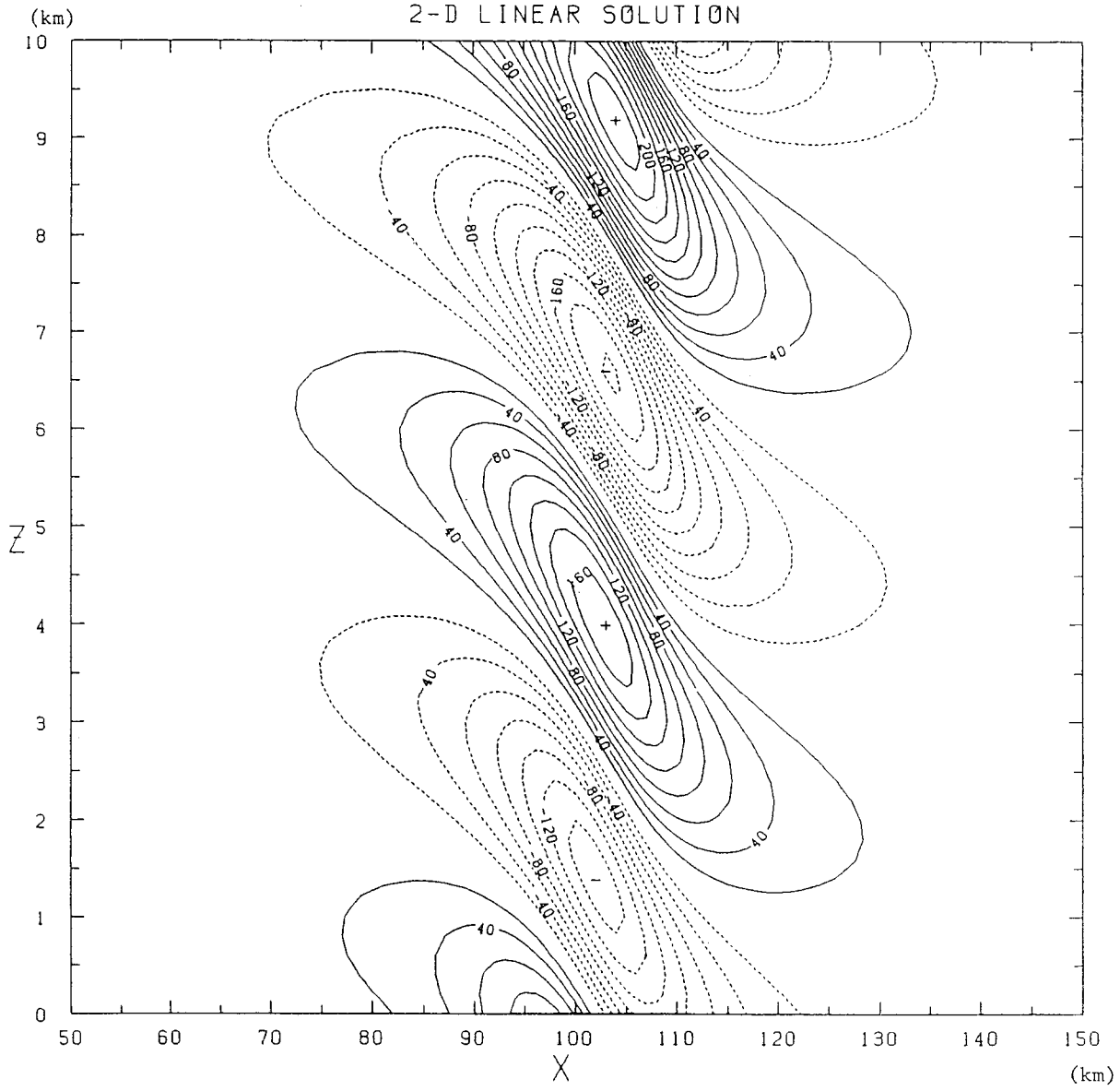

Fig. 2b. As in Fig. 2a, except the linear analytical solution.

our system (2.14)–(2.17) to derive conservative schemes, since the density is replaced by the pressure and potential temperature, and, in addition, the pressure and the potential temperature are divided into their means and deviations. We need the latter division to reduce the truncation error which contaminates the results rather quickly.

In conclusion, the author wishes to suggest an application of the variational grid generation. We can determine arbitrarily two parameters, λ_v, λ_o, and one function w. The λs represent the relative importance of the index integral as mentioned earlier, and w determines the grid-size variation of the model such that grid size becomes small when w is large and vice versa (see for example Brackbill and Saltzman 1982). We can therefore generate many types of grids by choosing w. If we formulate w into a time dependent form, an adaptive grid is obtained. As an example, choosing the form as

$$w = (\nabla u)^2 + (\nabla w)^2, \tag{17}$$

small meshes would be generated over the high-shear region and an effect like nested grid systems would be produced. Therefore, we will possibly be able to apply this variational generation technique to cases where nested systems are otherwise needed.

Acknowledgments

The author is indebted to T. Koide for introducing the grid generation technique to the author, and to F. Kimura and S. Takahashi for useful discussions and suggestions.

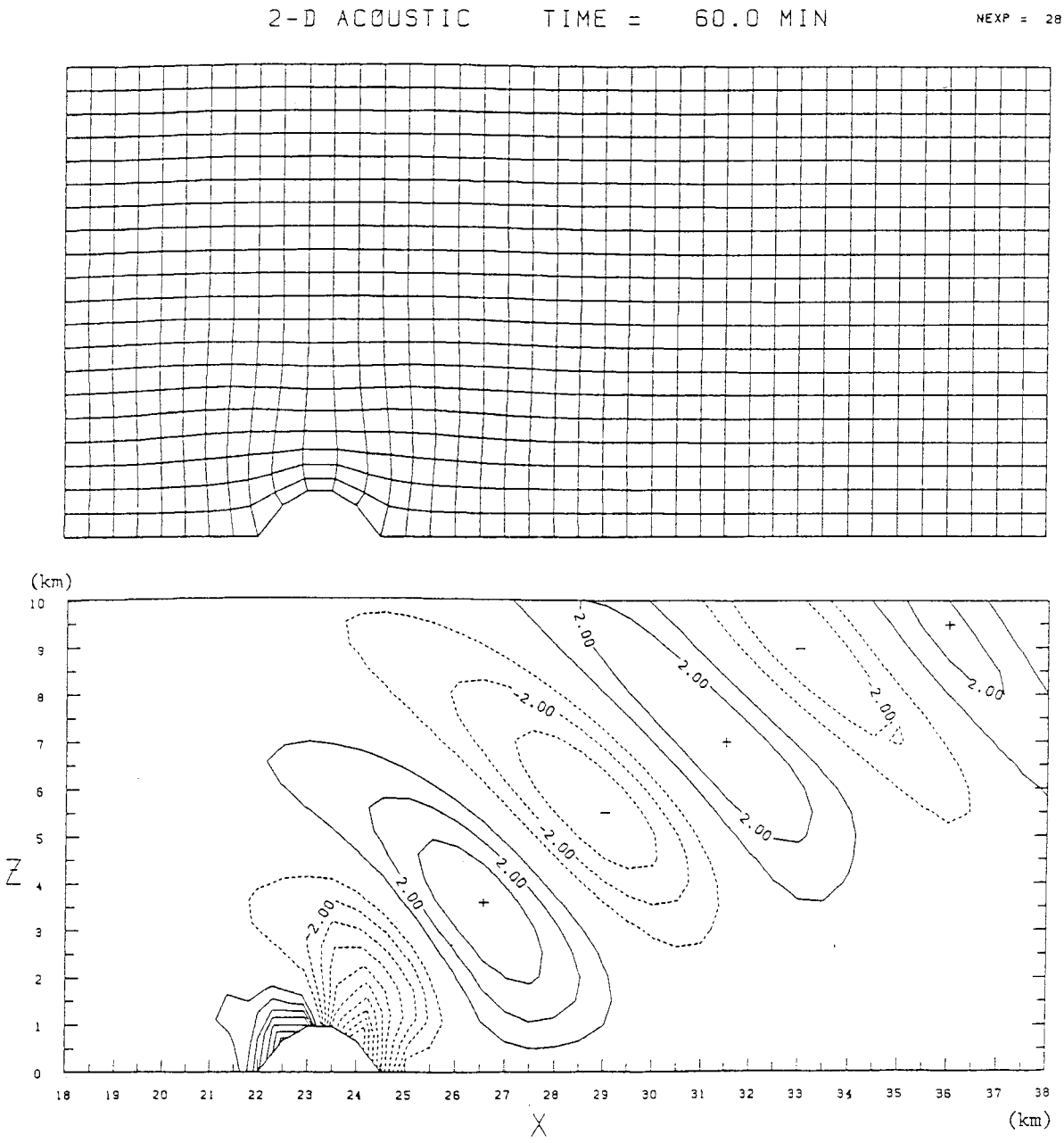

Fig. 3. Grid distribution generated by the variational method with λ_v=10, λ_o=10 (upper) and contours of vertical velocity (lower) for a semi-circular mountain with a radius of 1 km. The unit of velocity is 1 m/sec.

The computations were performed with the use of a HITAC S-810 and M-280 computers at MRI. The graphics is drawn by the NCAR graphic subroutines.

Appendix

Numerical aspects

a. Grid point distribution

As shown in Fig. FA1, all variables except the pressure (the Exner function) are located at the same points. The pressure is staggered in the vertical.

b. Finite difference schemes

Define Schuman-type operators (Schuman, 1962) as

$$\delta_\eta \phi = \frac{\phi(\eta + \Delta\eta/2) - \phi(\eta - \Delta\eta/2)}{\Delta\eta}, \qquad \text{(A.1)}$$

$$\bar{\phi}_\eta = \frac{\phi(\eta + \Delta\eta/2) + \phi(\eta - \Delta\eta/2)}{2}. \qquad \text{(A.2)}$$

Here ϕ denotes the dependent variable, η the independent variable, and $\Delta\eta$ is interval over which the operation takes place. The equations are, then, written as

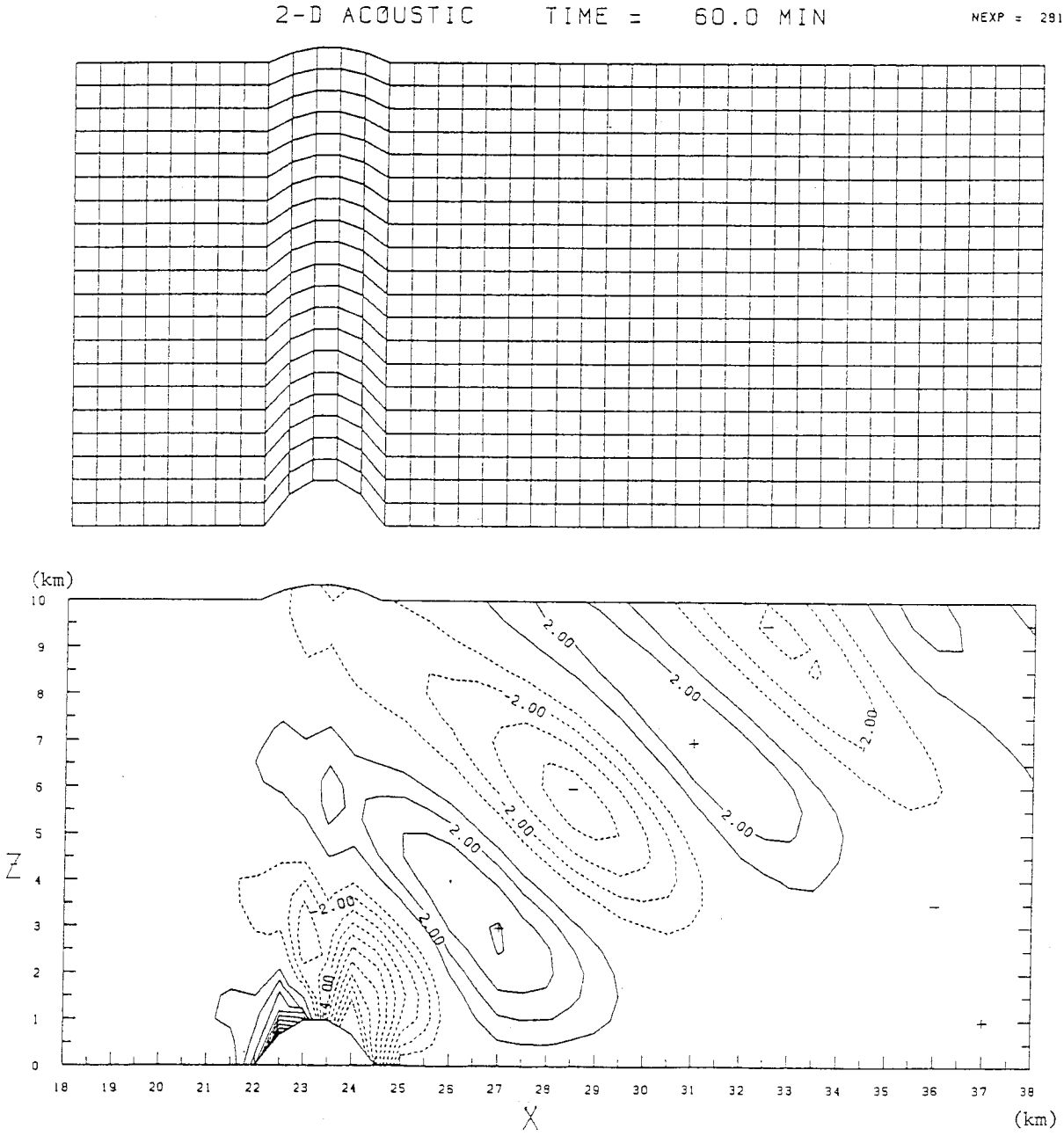

Fig. 4. As in Fig. 3, except in z* coordinates.

$$\begin{aligned}\delta_t \bar{u}^t &+ \hat{u}\delta_\xi \bar{u}^\xi + \hat{w}\delta_\zeta \bar{u}^\zeta \\ &+ c_p(\Theta+\theta)\frac{\partial \xi}{\partial x}\delta_\xi \bar{\pi}^{\xi\zeta} \\ &+ c_p\frac{\partial \zeta}{\partial x}(\theta\delta_\zeta \pi + \Theta\delta_\zeta \bar{\pi}^{2t}) = F_u, \qquad \text{(A.3)}\end{aligned}$$

$$\begin{aligned}\delta_t \bar{w}^t &+ \hat{u}\delta_\xi \bar{w}^\xi + \hat{w}\delta_\zeta \bar{w}^\zeta \\ &+ c_p(\Theta+\theta)\frac{\partial \xi}{\partial z}\delta_\xi \bar{\pi}^{\xi\zeta} \\ &+ c_p\frac{\partial \zeta}{\partial z}(\theta\delta_\zeta \pi + \Theta\delta_\zeta \bar{\pi}^{2t}) = F_w, \qquad \text{(A.4)}\end{aligned}$$

$$\delta_t \bar{\theta}^t + \hat{u}\delta_\xi \bar{\theta}^\xi + \hat{w}\delta_\zeta \bar{\theta}^\zeta = Q, \qquad \text{(A.5)}$$

$$\begin{aligned}\delta_t \bar{\pi}^t &+ \delta_\xi(\overline{\bar{\tilde{u}}^\zeta \pi}^\xi) + \delta_\zeta(\bar{\tilde{w}}^\zeta \pi) - (\delta_\xi \bar{\tilde{u}}^{\xi\zeta} + \delta_\zeta \hat{w}) \\ &- \frac{\bar{w}^\zeta}{H_s} + \frac{R_d(\Pi+\pi)}{c_v}\left\{\left.\frac{\partial \xi}{\partial x}\right|_\pi \delta_\xi \bar{u}^{\xi\zeta}\right. \\ &+ \left.\left.\frac{\partial \xi}{\partial z}\right|_\pi \delta_\xi \bar{w}^{\xi\zeta}\right\} + \frac{R_d}{c_v}\left\{\left.\frac{\partial \zeta}{\partial x}\right|_\pi \cdot(\pi\delta_\zeta u\right. \\ &+ \left.\Pi\delta_\zeta \bar{u}^{2t}) + \left.\frac{\partial \zeta}{\partial z}\right|_\pi \cdot(\pi\delta_\zeta w + \Pi\delta_\zeta \bar{w}^{2t})\right\} \\ &= \frac{R_d(\Pi+\pi)}{c_v(\Theta+\theta)}Q, \qquad \text{(A.6)}\end{aligned}$$

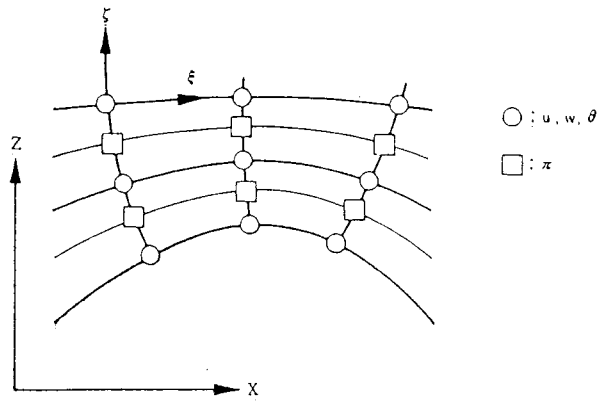

Fig. FA1. Grid point and variable distributions.

where the finite differences are centered in space and time,

$$\frac{\partial \xi}{\partial x} = \frac{1}{Det}\delta_\zeta \bar{z}^\zeta \ , \ \frac{\partial \xi}{\partial z} = -\frac{1}{Det}\delta_\zeta \bar{x}^\zeta, \tag{A.7a}$$

$$\frac{\partial \zeta}{\partial x} = -\frac{1}{Det}\delta_\xi \bar{z}^\xi \ , \ \frac{\partial \zeta}{\partial z} = -\frac{1}{Det}\delta_\xi \bar{x}^\xi, \tag{A.7b}$$

$$\left.\frac{\partial \xi}{\partial x}\right|_\pi = \frac{1}{Det_\pi}\delta_\zeta z \ , \ \left.\frac{\partial \xi}{\partial z}\right|_\pi = -\frac{1}{Det_\pi}\delta_\zeta x \ , \tag{A.8a}$$

$$\left.\frac{\partial \zeta}{\partial x}\right|_\pi = -\frac{1}{Det_\pi}\delta_\xi \bar{z}^{\xi\zeta} \ , \ \frac{\partial \zeta}{\partial z} = \frac{1}{Det_\pi}\delta_\xi \bar{x}^{\xi\zeta}, \tag{A.8b}$$

$$Det = \delta_\xi \bar{x}^\xi \cdot \delta_\zeta \bar{z}^\zeta - \delta_\zeta \bar{x}^\zeta \cdot \delta_\xi \bar{z}^\xi, \tag{A.9}$$

and

$$Det_\pi = \delta_\xi \bar{x}^\xi \cdot \delta_\zeta z - \delta_\zeta x \cdot \delta_\xi \bar{z}^\xi. \tag{A.10}$$

By using a semi-implicit time scheme in the ζ direction,it was sufficient to set, as an example, Δt=1sec for Δx=500 m regardless of the magnitude of Δz.

c. Numerical filter

A time filter proposed by Robert (1966) and Asselin (1972) is incorporated in the model to remove computational modes which are inevitable for the schemes using three time levels. This filter is described as follows:

$$\phi^t = \phi^{*^t} + \nu(\phi^{t-\Delta t} + \phi^{*^{t+\Delta t}} - 2\phi^{*^t}), \tag{A.11}$$

where ϕ^* is the value not yet smoothed. In the experiments presented in this paper, we used the coefficient ν=0.15.

In addition to the time filter, we used a 4th-order diffusion term in the ξ direction to damp very short wavelength modes because the subgrid mixing terms are very small in stable regions. It has the finite-difference form

$$-K_D\delta_{\xi\xi\xi\xi}\phi. \tag{A.12}$$

For the experiment presented here, we found

$$\frac{K_D\Delta t}{\Delta x^4} = 5 \times 10^{-4}$$

to be a satisfactory value.

References

Asselin, R., 1972: Frequency filter for time integrations. *Mon. Wea. Rev.*, 100, 487–490.

Brackbill, J.U. and J.S. Saltzman, 1982: Adaptive zoning for singular problems in two dimensions. *J. Comput. Phys.*, **46**, 342–368.

Clark, T.L., 1977: A small-scale dynamic model using a terrain-following coordinate transformation. *J. Comput. Phys.*, 24, 186–215.

Deardorff, J.W., 1972: Numerical investigation of neutral and unstable planetary boundary layers. *J. Atmos. Sci.*, **29**, 91–115.

Eiseman, P.R., 1982: Orthogonal grid generation. *Numerical Grid Generation,* Thompson, J. F. (Ed.), *Appl. Math. Comput.*, 10/11, 192–233.

Gal-Chen, T. and R.C.J. Somerville, 1975: On the use of a coordinate transformation for the solution of the Navier-Stokes equations. *J. Comput. Phys.*, **17**, 209–228.

Klemp, J.B. and D.K. Lilly, 1978: Numerical simulation of hydrostatic mountain waves. *J. Atmos. Sci.*, **35**, 78–107.

Lilly, D.K., 1962: On the numerical simulation of buoyant convection. *Tellus*, 14, 148–172.

Long, R.R., 1955: Some aspects of the flow of stratified fluids. III. Continuous density gradients. *Tellus*, 7, 341–357.

Miles, J.W. and H.E. Huppert, 1968: Lee waves in a stratified flow. Part 2. Semi-circular obstacle. *J. Fluid Mech.*, **33**, 803–814.

Orlanski, I., 1976: A simple boundary condition for unbounded hyperbolic flows. *J. Comput. Phys.*, 21, 251–269.

Phillips, N.A., 1957: A coordinate system having some special advantages for numerical forecasting. *J. Meteor.*, 14, 184–185.

Pielke, R.A., 1984: *Mesoscale meteorological modeling.* Academic Press. 612 pp.

Robert, A.J., 1966: The integration of a low order spectral form of the primitive meteorological equations. *J. Meteor. Soc. Japan*, 44, 237–245.

Ryskin, G. and L.G. Leal, 1983: Orthogonal mapping. *J. Comput. Phys.*, **50**, 71–100.

Sahasi, K., 1981: Numerical experiment of land sea breeze circulation with undulating orography. Part I. *J. Meteor. Soc. Japan*, 59, 361–372.

Sharman, R.D., T.L. Keller and M.G. Wurtele, 1988: Incompressible and anelastic flow simulations on numerically generated grids. *Mon. Wea. Rev.*, **116**, 1124–1136.

Shuman, F.G., 1962: Numerical experiments with the primitive equations. *Proceedings of the Interna-*

tional Symposium on Numerical Weather Prediction in Tokyo,1960. Meteor. Soc. Japan, 85–107.

Thompson, J.F., 1984: Grid generation techniques in computational fluid dynamics. *AIAA Journal*, **22**, 1505–1523.

Thompson, J.F., Z.U.A. Warsi and C.W. Mastin,1982: Boundary-fitted coordinate systems for numerical solution of partial differential equations-A review. *J. Comput. Phys.*, **47**, 1–108.

Thompson, J.F., Z.U.A. Warsi and C.W. Mastin, 1985: *Numerical grid generation. Foundations and applications.* North-Holland. 483 pp.

数値的に生成された格子による圧縮流体のシミュレーション

里村雄彦

(気象研究所)